

Whole-Body Biodistribution and Radiation Dosimetry of ^{18}F -GE067: A Radioligand for In Vivo Brain Amyloid Imaging

Michel Koole¹, Dewi M. Lewis², Christopher Buckley², Natalie Nelissen³, Mathieu Vandebulcke⁴, David J. Brooks^{2,5}, Rik Vandenberghe^{3,6}, and Koen Van Laere¹

¹Nuclear Medicine, University Hospital and K.U. Leuven, Leuven, Belgium; ²GE Healthcare Medical Diagnostics Research and Development, Amersham, United Kingdom; ³Laboratory for Cognitive Neurology, K.U. Leuven, Leuven, Belgium; ⁴Psychiatry Department, UZ Leuven, Leuven, Belgium; ⁵Division of Neuroscience, Faculty of Medicine, Imperial College London, London, United Kingdom; and ⁶Neurology Department, UZ Leuven, Leuven, Belgium

We have characterized the biodistribution and dosimetry of ^{18}F -3'-F-6-OH-BTA1 (^{18}F -GE067), a newly developed radioligand to visualize and quantify amyloid burden, in healthy elderly human subjects. **Methods:** Six subjects (5 men and 1 woman; age range, 51–74 y) underwent dynamic whole-body PET/CT for 6 h after a bolus injection of ^{18}F -GE067. Source organs were delineated on PET/CT. Individual organ doses and effective doses were determined. **Results:** No adverse events or clinically significant changes were observed. ^{18}F -GE067 is excreted predominantly through the hepatobiliary system. The gallbladder, upper large intestine, and small intestine are the organs with the highest absorbed dose (average, 287, 173, and 155 $\mu\text{Gy}/\text{MBq}$, respectively). The mean effective dose was $33.8 \pm 3.4 \mu\text{Sv}/\text{MBq}$, a dose comparable to that of many other ^{18}F -labeled radiopharmaceuticals. **Conclusion:** The estimated effective dose of ^{18}F -GE067 for PET amyloid imaging was acceptable (class II-b defined by the World Health Organization), and relatively low variability between subjects was observed.

Key Words: amyloid imaging; ^{18}F -GE067; PET; dosimetry; biodistribution; healthy subjects

J Nucl Med 2009; 50:818–822

DOI: 10.2967/jnumed.108.060756

Alzheimer disease (AD) affects 7% of the general population older than 65 y and 30% of those older than 80 y (1). According to a meta-analysis of a prospective clinicopathologic series conducted in academic memory clinics, the sensitivity of a diagnosis of clinically probable AD is 0.65 (± 0.15 SD) and specificity is 0.76 (± 0.20). If clinically probable and possible AD are combined, the sensitivity is 0.90 (± 0.07), but specificity drops to 0.56 (± 0.22) (2). It has been proposed that, at least in the setting of clinical research studies and drug development, biomarkers such as the imaging of amyloid β (A β) by PET and cerebrospinal fluid

analysis of A β and tau proteins should be included in new diagnostic criteria for AD, to increase the accuracy and allow earlier interventions of disease-modifying strategies (3).

In vivo imaging of A β in the brain using PET and SPECT has been successful with ^{11}C -labeled compounds such as ^{11}C -Pittsburgh compound B (^{11}C -PIB) (4), ^{11}C -4-*N*-methylamino-4'-hydroxystilbene (5), and ^{11}C -2-(2-[2-dimethylaminothiazol-5-yl]ethenyl)-6-(2-[fluoro]ethoxy)benzoxazole (6) but less so with ^{123}I -labeled compounds such as ^{123}I -6-iodo-2-(4'-dimethylamino-)phenyl-imidazo[1,2-*a*]pyridine (^{123}I -IMPY) (7). ^{11}C -PIB shows a 2-fold increase in cortical signal in probable AD patients versus controls, and neuropathologic studies have confirmed that regional ^{11}C -PIB binding in vivo correlates with levels of A β measured after death (8). However, only a few centers equipped with an on-site cyclotron are able to perform ^{11}C -based ligand studies. ^{18}F -based amyloid imaging agents would make in vivo imaging of A β more available for routine clinical use and allow longitudinal studies across multiple centers. So far, four ^{18}F -labeled ligands for use in humans are being developed. ^{18}F -(2-(1-{6-[(2-[^{18}F]fluoroethyl)(methyl)amino]-2-naphthyl}ethylidene) (^{18}F -FDDNP) is a naphthol, which labels both plaques and tangles in the brain but has a low specific signal (9). ^{18}F -4-(*N*-methylamino)-4'-(2-(2-(2-fluoroethoxy)ethoxy)ethoxy)stilbene and ^{18}F -AV45 are stilbene derivatives, selective for A β , and show an uptake pattern similar to ^{11}C -PIB (10).

Here we have characterized the safety, biodistribution, and radiation dosimetry of a novel ^{18}F -labeled benzothiazole compound selective for human A β , ^{18}F -3'-F-6-OH-BTA1 (^{18}F -GE067), a structural thioflavin analog of ^{11}C -PIB, in a study involving 6 healthy elderly human subjects. ^{18}F -GE067 allows in vivo PET of amyloid deposits in the AD brain (N. Nelissen, K. Van Laere, L. Thurfjell, et al., unpublished data, 2009).

MATERIALS AND METHODS

Healthy Subjects

Healthy subjects were recruited as part of a phase I PET study sponsored by GE Healthcare Ltd. and in response to an adver-

Received Dec. 3, 2008; revision accepted Feb. 5, 2009.

For correspondence or reprints contact: Koen Van Laere, Division of Nuclear Medicine, University Hospital Gasthuisberg, Herestraat 49, 3000 Leuven, Belgium.

E-mail: koen.vanlaere@uzleuven.be

COPYRIGHT © 2009 by the Society of Nuclear Medicine, Inc.

tisement in a local community newspaper. Six healthy Caucasian subjects (5 men; 1 woman; age range, 51–74 y) were included in the study. Demographic data for these subjects are summarized in Table 1. The subjects did not have any clinically significant medical or neurologic condition, and they did not have any clinically significant abnormality on physical, neurologic, or laboratory examinations. In addition, they did not have a first-degree relative with a diagnosis of AD. The study was approved by the local Ethics Committee, and written informed consent was obtained from all the volunteers before the study started.

Radiotracer Characteristics and Preparation

The investigational medicinal product ^{18}F -GE067 was batch-manufactured according to Good Manufacturing Guidelines, Eudralex volume 4, Annex 3 (11), at the Cyclotron Research Centre, University of Liege, Belgium, using a TracerLab-FX_{F-N} (GE Healthcare) chemistry platform. The chemical and radiochemical purity of the test item was assessed by analytic high-performance liquid chromatography system equipped with an ultraviolet and radioactivity detector. The total unlabeled GE067 chemical content was $0.7 \pm 0.3 \mu\text{g/mL}$, and the radiochemical purity was $98.1\% \pm 1.2\%$. The identity of the radiolabeled product was confirmed by coelution on high-performance liquid chromatography of a cold analytic standard of GE067.

^{18}F -GE067 was supplied as a ready-to-inject solution with a maximum of 10 μg of cold GE067 per dose; the solution for injection contained 7% ethanol (v/v) and 0.5% polysorbate 80 (w/v) in phosphate buffer (0.015 M).

PET/CT Procedure

Subjects received on average 121 MBq (range, 96–147 MBq) of ^{18}F -GE067 as a slow intravenous bolus injection (~ 10 s) through a catheter in an antecubital vein. A dynamic series of whole-body PET emission scans was obtained as described previously (12).

All subjects were scanned with a PET/CT camera (HiRez Biograph16; Siemens) at 3 consecutive times. For the first 90 min, 8 sequential whole-body scans from the midfemoral position to the head were obtained. During the other 2 times, single whole-body scans were obtained at about 160 and 260 min after injection. A low-dose (tube potential, 80 kV; effective mAs, 11), no-contrast, whole-body CT scan was obtained at the beginning of each time. The additional radiation burden of this low-dose CT was 0.5 mSv per whole-body scan.

Urine samples were collected and counted between scanning times, up to 6 h after injection ($n = 5/\text{subject}$).

Images from the HiRez Biograph16 were reconstructed using a 3-dimensional ordered-subset expectation maximization iterative algorithm (5 iterations and 8 subsets) and postsmoothed with a

3-dimensional gaussian filter (6-mm full width at half maximum). Reconstruction included model-based scatter as well as attenuation correction based on the measured CT-attenuation map.

Volumes of Interest (VOI)

Data transfer, VOI definition, and processing to calculate time–activity curves were performed as described previously using PMOD software (version 2.9; PMOD Inc.) (12). The following organs showed significant tracer accumulation and were included in the VOI template: brain, gallbladder, small intestine, heart, kidneys, liver, lungs, axial bone marrow, spleen, thyroid, and urinary bladder.

Residence Time and Absorbed Dose Calculations

Residence times were computed and normalized to injected activities by calculating the area under the time–activity curve of each organ. This was done using curve fitting to the time–activity curves as the primary method. The uptake in the brain, heart, liver, kidneys, red marrow, lungs, spleen, and remainder could be modeled with the following function:

$$\sum_i [A_i \times (1 - \exp(-\ln(2) \times t / \tau_{u,i})) \times \exp(-\ln(2) \times t / \tau_{e,i})],$$

where $i = 1-3$, A_i was a scaling parameter, $\tau_{u,i}$ represented the uptake time parameters, and $\tau_{e,i}$ represented the excretion time parameters. The model was fitted to the data by least-squares constraint minimization. Small intestine time–activity curves for 2 subjects and the gallbladder and thyroid time–activity curves in all subjects were not satisfactorily described by kinetic modeling. The curve fitting for these subjects and organs did not converge to an acceptable solution, even by changing the start estimates over a large representative range. For the intestine, accumulated activity entering the intestines at the last 2 times did not approximate the final fraction closely enough for unique fitting solutions. For the gallbladder, large variability in the measured values was encountered. In these subjects and organs, values based on the trapezoid rule were used, and the area under the curve after the acquisition of the last image was calculated by assuming only physical decay of ^{18}F and no additional biologic clearance to be conservative. Previously, we have shown that the calculation of the area under the curve using the trapezoid method gives a good approximation of the residence time (12).

The absorbed doses reported were calculated using OLINDA (Vanderbilt University), and the effective dose (ED) was calculated from the individual organ doses on the basis of a predefined weighting factor for each of the source organs (13).

The residence times for the upper large intestine (ULI), lower large intestine (LLI), and small intestine were calculated in 2 ways. For the 4 subjects in whom the fraction of injected activity

TABLE 1. Subject Data, Net Injected Activity of ^{18}F -GE067, and Individual Effective Dose Estimates

Subject no.	Sex	Age (y)	Height (m)	Mass (kg)	Body mass index (kg/m ²)	Injected dose (MBq)	Individual effective dose ($\mu\text{Sv}/\text{MBq}$)
1	M	74	165	63.0	23.1	95.8	30.7
2	M	51	172	69.5	23.5	97.2	33.3
3	F	71	153	58.0	24.8	139.1	37.5
4	M	73	160	71.0	27.8	144.0	29.4
5	M	56	188	81.0	22.9	146.5	37.4
6	M	63	174	80.0	26.4	105.1	34.5
Mean \pm SD		64.7 \pm 8.8	168.7 \pm 11.2	70.4 \pm 8.3	24.8 \pm 1.8	121.3 \pm 22.2	33.8 \pm 3.36

entering the small intestine could be estimated accurately, we used the International Commission on Radiological Protection (ICRP) 30 (14) gastrointestinal model as incorporated in OLINDA, using the fraction entering the small intestine as input (calculated from the kinetic modeling of the intestinal VOI time–activity curves). This value was set equal to the largest decay-corrected fraction of injected activity encompassed by the intestinal region of interest.

For the 2 subjects in whom no accurate estimate of the fraction injected activity could be made, we also used a predefined distribution of residence times—50% for the small intestine, 25% for the ULI, and 25% for the LLI—which is a good approximation for slowly excreted tracers (12). For the 4 subjects in whom small, ULI, and LLI parameter fitting was possible, the average retention time calculated with the trapezoid method was slightly lower than the kinetically modeled values and resulted in ED estimates that were 5% lower, indicating that the trapezoid approach is appropriate for quantifying organ ^{18}F -GE067 uptake.

The updated dynamic bladder model (13) was used to calculate dose to the bladder wall, with a bladder voiding interval of 2 h. The fraction of activity excreted through the bladder and the corresponding biologic half-life were based on the accumulated activity excreted at all voiding moments between and after scans. For this purpose $A \times (1 - \exp(-\ln(2) \times t/\tau_u))$ was fitted to the cumulative activity values, where τ_u was the biologic decay and A was the fraction of activity released from the body during voiding between scan sequences.

RESULTS

During these studies, no adverse events were reported. All monitored clinical parameters (heart rate, blood pressure, respiration rate, body temperature, 12-lead electrocardiogram) stayed normal during and after scanning. No clinically significant adverse experiences were reported by the subjects at the time of scanning, nor were any reported during the follow-up phone interview 24 h after the scan.

Figure 1 shows an exemplary series of whole-body slices of ^{18}F -GE067 over time for subject 1 (Table 1). The tracer is readily taken up in the brain and liver and quickly excreted in the gastrointestinal system. Urinary tract activity is noted after a few minutes.

Figure 2 shows slices through the brain of a representative healthy subject and a patient with AD from the subsequent phase I study with ^{18}F -GE067.

Supplemental Table 1 (supplemental materials are available online only at <http://jnm.snmjournals.org>) shows cal-

culated residence times. The highest variability in residence times was observed for the small intestine and gallbladder. The mean residence time for the gallbladder for all subjects was 0.16 ± 0.011 h, with the lowest value of 0.014 h and the highest value 0.312 h.

Figure 3 shows decay-corrected relative time–activity curves for the brain, liver, small intestine, gallbladder, and urinary bladder after injection of ^{18}F -GE067. Up to 20% of the injected activity is excreted through the urinary tract; the remainder is eliminated through the gastrointestinal tract.

Table 2 summarizes the individual organ doses and individual ED results for all subjects and the means and SD. The gallbladder wall is the dose-limiting organ, with the highest organ dose of 0.287 mGy/MBq. For a standard injected activity of 185 MBq, no individual organ dose would, therefore, exceed 200 mGy. A high variability in the gallbladder organ-absorbed dose, between 0.051 and 0.520 mGy/MBq (SD, 0.164 mGy/MBq), was observed.

Table 1 includes the individual ED estimates for all subjects. The average ED was 33.8 $\mu\text{Sv}/\text{MBq}$ (range, 29.4–37.5 $\mu\text{Sv}/\text{MBq}$). No significant difference in ED was found between the 5 men and 1 woman in the study, and no changes were observed within the small age range of participating subjects.

DISCUSSION

Our dosimetry studies on ^{18}F -GE067 have resulted in an ED estimate for the tracer of 33.8 $\mu\text{Sv}/\text{MBq}$. The subjects participating in this study received a total ED of 4.12 ± 0.96 mSv for the PET and 1.5 mSv for the CT parts. Compared with other ^{18}F -labeled radiopharmaceuticals with typical ED values in the range of 20–35 $\mu\text{Sv}/\text{MBq}$, ^{18}F -GE067 has a radiation burden in the upper range.

The observed distribution pattern of ^{18}F -GE067 shows predominant hepatobiliary excretion and is similar to that observed for its structural analog ^{11}C -PIB, with a near-identical fraction ($\sim 20\%$) of urinary excretion (estimated ED for ^{11}C -PIB, 4.7 ± 0.8 $\mu\text{Sv}/\text{MBq}$) (15). Another human study in 6 subjects by O’Keefe et al. (16) found comparable values resulting in an ED estimate of 5.3 $\mu\text{Sv}/\text{MBq}$. Our own measurement in 2 healthy male subjects (age, 20–30 y) (K. Van Laere, written communication, local ethics committee approval report, 2006), using the same methodology as is used in the current work, resulted in 4.8 $\mu\text{Sv}/\text{MBq}$.

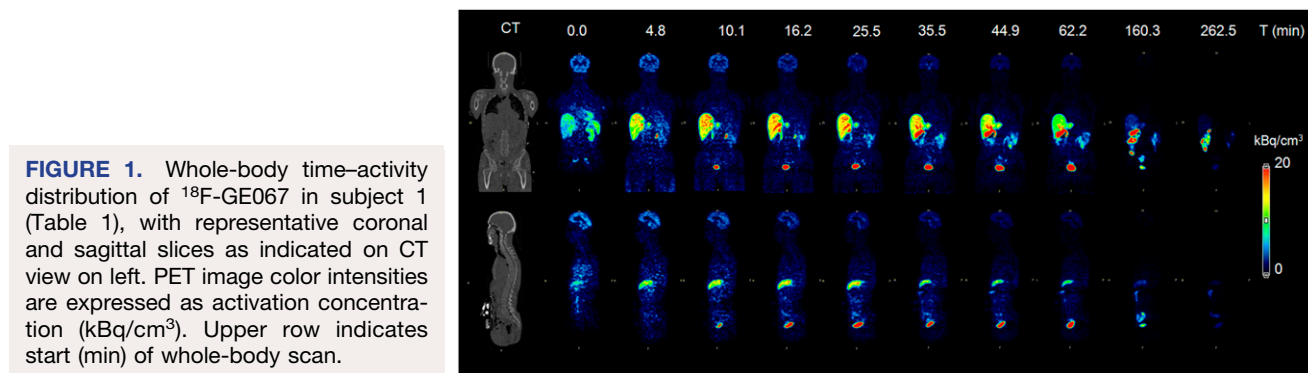


FIGURE 1. Whole-body time–activity distribution of ^{18}F -GE067 in subject 1 (Table 1), with representative coronal and sagittal slices as indicated on CT view on left. PET image color intensities are expressed as activation concentration (kBq/cm^3). Upper row indicates start (min) of whole-body scan.

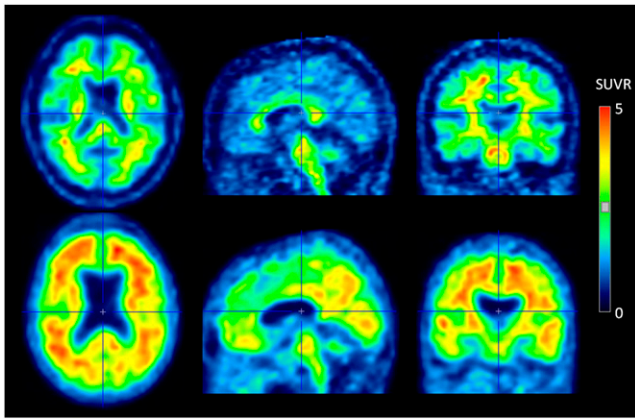


FIGURE 2. Brain uptake distribution of ^{18}F -GE067 in healthy 64-y-old male subject (top), compared with 68-y-old male AD patient (bottom). Transverse, sagittal, and coronal sections indicate absence of specific gray matter uptake of ^{18}F -GE067 and aspecific uptake in white matter, pons, and thalamus. Images represent standardized uptake value ratios (SUVR) to cerebellar cortex, between 85 and 105 min after injection, obtained from phase I clinical study.

This result confirmed that over various centers, dosimetry estimates are consistent despite some methodologic differences in source organ determination and delineation and indicated that current values for ^{18}F -GE067 are robust, despite some reports having warned for methodologic differences in

determination of and assumptions concerning source organ residence time distribution that may give rise to appreciable differences (17).

The dosimetry of ^{18}F -BAY94-9172 in 3 subjects has been described in abstract form by O’Keefe et al. and was low for an ^{18}F -labeled ligand: $14.7 \pm 1.4 \mu\text{Sv}/\text{MBq}$ (16). Internal dosimetry data for ^{18}F -FDDNP in humans are not available in the literature at this point. Radiation burden per injected activity for ^{123}I -IMPY is higher than for the ^{18}F ligands, with an estimated ED of $42 \mu\text{Sv}/\text{MBq}$ (18).

Although the current estimates were obtained in elderly cognitively intact healthy subjects, none of whom showed evidence of specific increased brain uptake levels indicating amyloid deposition (which has been found in 20%–30% of healthy elderly populations (19,20)), these data can be extrapolated to pathologic brains. Assuming a conservative 3-fold brain uptake (as a maximum value of the specific uptake increase observed in AD cases) (N. Nelissen, K. Van Laere, L. Thurfjell, et al., unpublished data, 2009) and corresponding increase in residence time for the brain, with unaltered tracer whole-body distribution and excretion, we calculated the influence on total ED. This assumption would augment the ED estimate by less than 1%, to $34.0 \mu\text{Sv}/\text{MBq}$, because the brain is incorporated in the remainder of the body and does not contribute significantly to the ED. Without medication effects that would induce altered hepatic metabolism of the tracer (e.g., enzyme

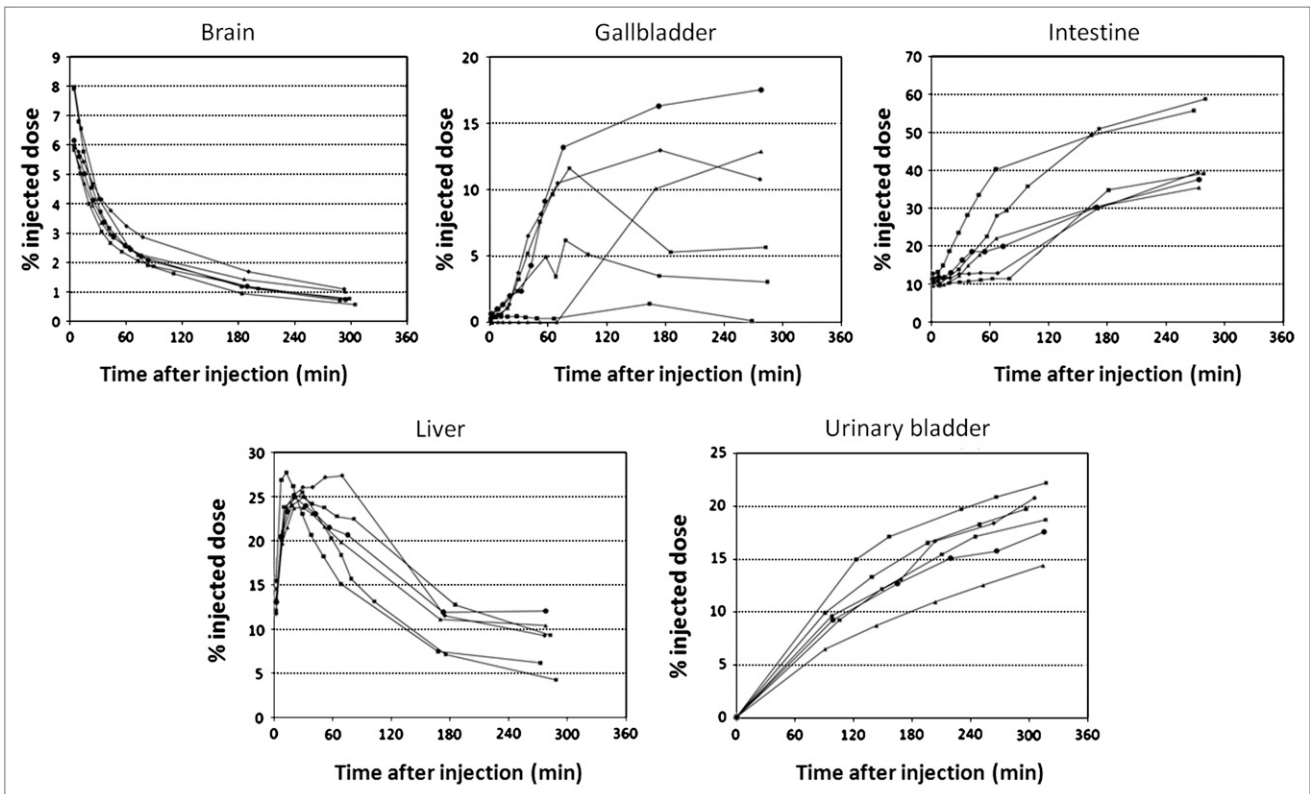


FIGURE 3. Mean activity in brain, gallbladder, intestine, liver, and urinary bladder as fraction of total-body activity, at all time points for 6 subjects.

TABLE 2. Radiation Absorbed Dose Estimates (OLINDA) Based on ICRP 30 (13) Gastrointestinal Tract Model

Organ	Dose estimate (mGy/MBq)	Coefficient of variation (%)
Adrenals	1.46E-02 ± 2.35E-03	16.1
Brain	1.19E-02 ± 1.18E-03	9.9
Breasts	5.59E-03 ± 1.05E-03	18.8
Gallbladder wall	2.87E-01 ± 1.64E-01	57.1
LLI wall	8.15E-02 ± 1.51E-02	18.5
Small intestine	1.55E-01 ± 6.19E-02	39.9
Stomach wall	1.52E-02 ± 2.84E-03	18.7
ULI wall	1.73E-01 ± 7.22E-02	41.7
Heart wall	1.21E-02 ± 2.44E-03	20.2
Kidneys	4.01E-02 ± 5.77E-03	14.4
Liver	6.39E-02 ± 1.12E-02	17.5
Lungs	1.67E-02 ± 1.63E-03	9.8
Muscle	9.7E-03 ± 1.48E-03	15.3
Ovaries	3.31E-02 ± 8.59E-03	26.0
Pancreas	1.72E-02 ± 2.91E-03	16.9
Red marrow	1.53E-02 ± 1.63E-03	10.7
Osteogenic cells	1.27E-02 ± 2.15E-03	16.9
Skin	5.54E-03 ± 9.01E-04	16.3
Spleen	1.59E-02 ± 3.06E-03	19.2
Testes	5.30E-03 ± 2.61E-03	49.2
Thymus	6.25E-03 ± 1.28E-03	20.5
Thyroid	6.56E-03 ± 1.96E-03	29.9
Urinary bladder	6.16E-02 ± 6.61E-03	10.7
Uterus	2.72E-02 ± 6.75E-03	24.8
Total body	1.36E-02 ± 2.03E-03	14.9
Effective dose (mSv/MBq)	0.0338 ± 0.0034	10.1

Data are mean ± SD.

induction), the ED calculation is, thus, also valid for patient populations with mild cognitive impairment and AD.

The gallbladder wall was the dose-limiting organ, and a large variability in gallbladder activity was found due to large differences in the individual kinetics of gallbladder emptying, a process influenced by multiple hormonal factors and gastrointestinal interactions.

The average injected tracer mass dose in this study was 10 µg of ¹⁸F-GE067 and did not produce any subjective or clinically meaningful changes in laboratory blood tests, blood pressure, pulse, and respiration rate in any subject. No adverse events were reported in this study. Therefore, in this pilot study ¹⁸F-GE067 also appears to be safe from a pharmacologic standpoint. In view of the limited number of investigated subjects in the current study, further safety data will be collected during the development of the radiopharmaceutical for regulatory submission.

CONCLUSION

The administration of ¹⁸F-GE067 is safe and leads to a reasonable radiation burden to investigated subjects. This result is quantitatively in line with the results of many other ¹⁸F-labeled radioligand studies and thus falls into an ICRP/World Health Organization class II-b category for standard injected activity (185 MBq or less in view of the more than

sufficient image quality) in central nervous system imaging to determine amyloid load in the brain.

ACKNOWLEDGMENTS

We thank Stijn Dirix, Hendrikje Jeandarme, Carine Schildermans, and Mieke Soons for their contributions and the PET departments of the University Hospitals Leuven and of the Cyclotron Research Centre Liege. After the time that the manuscript for this paper was accepted, ¹⁸F-GE067 was granted an INN name, ¹⁸F-flutemetamol.

REFERENCES

1. Blennow K, de Leon MJ, Zetterberg H. Alzheimer's disease. *Lancet*. 2006; 368:387–403.
2. Gay BE, Taylor KI, Hohl U, Tolnay M, Staehelin HB. The validity of clinical diagnoses of dementia in a group of consecutively autopsied memory clinic patients. *J Nutr Health Aging*. 2008;12:132–137.
3. Dubois B, Feldman HH, Jacova C, et al. Research criteria for the diagnosis of Alzheimer's disease: revising the NINCDS-ADRDA criteria. *Lancet Neurol*. 2007;6:734–746.
4. Klunk WE, Engler H, Nordberg A, et al. Imaging brain amyloid in Alzheimer's disease with Pittsburgh Compound-B. *Ann Neurol*. 2004;55:306–319.
5. Verhoeff NP, Wilson AA, Takeshita S, et al. In-vivo imaging of Alzheimer disease beta-amyloid with [¹¹C]SB-13 PET. *Am J Geriatr Psychiatry*. 2004;12:584–595.
6. Kudo Y, Okamura N, Furumoto S, et al. 2-(2-[2-dimethylaminothiazol-5-yl]ethenyl)-6-(2-[fluoro]ethoxy)benzoxazole: a novel PET agent for in vivo detection of dense amyloid plaques in Alzheimer's disease patients. *J Nucl Med*. 2007;48:553–561.
7. Kung MP, Hou C, Zhuang ZP, Skovronsky D, Kung HF. Binding of two potential imaging agents targeting amyloid plaques in postmortem brain tissues of patients with Alzheimer's disease. *Brain Res*. 2004;1025:98–105.
8. Ikonovic MD, Klunk WE, Abrahamson EE, et al. Post-mortem correlates of in vivo PiB-PET amyloid imaging in a typical case of Alzheimer's disease. *Brain*. 2008;131:1630–1645.
9. Small GW, Kepe V, Ercoli LM, et al. PET of brain amyloid and tau in mild cognitive impairment. *N Engl J Med*. 2006;355:2652–2663.
10. Rowe CC, Ackerman U, Browne W, et al. Imaging of amyloid beta in Alzheimer's disease with ¹⁸F-BAY94-9172, a novel PET tracer: proof of mechanism. *Lancet Neurol*. 2008;7:129–135.
11. European Commission on Enterprise and Industry. *EudraLex (The Rules Governing Medicinal Products in the European Union): Volume 3—Scientific Guidelines for Medicinal Products for Human Use*. Available at: http://ec.europa.eu/enterprise/pharmaceuticals/eudralex/vol3_en.htm. Accessed March 30, 2009.
12. Van Laere K, Koole M, Sanabria Bohorquez SM, et al. Whole-body biodistribution and radiation dosimetry of the human cannabinoid type-1 receptor ligand ¹⁸F-MK-9470 in healthy subjects. *J Nucl Med*. 2008;49:439–445.
13. International Commission on Radiological Protection (ICRP). *ICRP Publication 60: 1990 Recommendations of the International Commission on Radiological Protection*. Oxford, U.K.: Pergamon Press; 1991.
14. International Commission on Radiological Protection (ICRP). *ICRP Publication 30, Part 1: Limits for Intakes of Radionuclides by Workers*. Oxford, U.K.: Pergamon Press; 1979.
15. Scheinin NM, Tolvanen TK, Wilson IA, Arponen EM, Nagren KA, Rinne JO. Biodistribution and radiation dosimetry of the amyloid imaging agent ¹¹C-PiB in humans. *J Nucl Med*. 2007;48:128–133.
16. O'Keefe GJ, Saunderson TH, Ng S, et al. Radiation dosimetry of β-amyloid tracers ¹¹C-PiB and ¹⁸F-BAY94-9172. *J Nucl Med*. 2009;50:309–315.
17. Sprague DR, Chin FT, Liow JS, et al. Human biodistribution and radiation dosimetry of the tachykinin NK1 antagonist radioligand [¹⁸F]SPA-RQ: comparison of thin-slice, bisected, and 2-dimensional planar image analysis. *J Nucl Med*. 2007;48:100–107.
18. Newberg AB, Wintering NA, Plossl K, et al. Safety, biodistribution, and dosimetry of ¹²³I-IMPY: a novel amyloid plaque-imaging agent for the diagnosis of Alzheimer's disease. *J Nucl Med*. 2006;47:748–754.
19. Nelissen N, Vandenbulcke M, Fannes K, et al. Aβ amyloid deposition in the language system and how the brain responds. *Brain*. 2007;130:2055–2069.
20. Villemagne VL, Pike KE, Darby D, et al. Aβ deposits in older non-demented individuals with cognitive decline are indicative of preclinical Alzheimer's disease. *Neuropsychologia*. 2008;46:1688–1697.